Nanometer-scale compositional variations in III-V semiconductor heterostructures characterized by scanning tunneling microscopy

E. T. Yu,[a] S. L. Zuo, W. G. Bi, and C. W. Tu
Department of Electrical and Computer Engineering, University of California at San Diego, LaJolla, California 92093-0407

A. A. Allerman and R. M. Biefeld
Sandia National Laboratories, Albuquerque, New Mexico 87185

(Received 13 October 1998; accepted 22 March 1999)

Nanometer-scale compositional structure in $InAs_xP_{1-x}/InN_yAs_xP_{1-x-y}$//InP heterostructures grown by gas-source molecular beam epitaxy and in $InAs_{1-x}P_x/InAs_{1-y}Sb_y$/InAs heterostructures grown by metalorganic chemical vapor deposition has been characterized using cross-sectional scanning tunneling microscopy. $InAs_xP_{1-x}$ alloy layers are found to contain As-rich and P-rich clusters with boundaries formed preferentially within $(\bar{1}11)$ and $(1\bar{1}1)$ crystal planes. Similar compositional clustering is observed within $InN_yAs_xP_{1-x-y}$ alloy layers. Imaging of $InAs_{1-x}P_x/InAs_{1-y}Sb_y$ superlattices reveals nanometer-scale clustering within both the $InAs_{1-x}P_x$ and $InAs_{1-y}Sb_y$ alloy layers, with preferential alignment of compositional features in the $[\bar{1}12]$ direction. Instances are observed of compositional features correlated across a heterojunction interface, with regions whose composition corresponds to a smaller unstrained lattice constant relative to the surrounding alloy material appearing to propagate across the interface. © *1999 American Vacuum Society.* [S0734-2101(99)15204-7]

I. INTRODUCTION

Features in the atomic-scale structure of alloys and of heterojunction interfaces can exert a profound influence on electronic, optical, and transport properties in semiconductor heterostructure materials and devices. Atomic ordering, for example, which has been observed for a wide range of semiconductor alloys,[1–7] is known to produce significant reductions in energy band gaps of ordered alloys compared to those in corresponding random alloys.[8–11] Clustering and phase separation,[12–17] as well as spontaneous compositional modulation,[18,19] can directly affect carrier confinement, transport, and optical properties of alloys and quantum-confined structures. Characterization of atomic-scale compositional structure and its correlation with epitaxial growth conditions and with material and device characteristics is, consequently, an essential aspect of semiconductor heterostructure material and device engineering.

Among the numerous methods used to perform characterization of materials at the atomic to nanometer scale, scanning probe techniques have emerged as extremely powerful tools for investigation of structural, compositional, electronic, optical, and magnetic properties with extremely high spatial resolution. For investigation of the atomic-scale alloy layer and interface structure in III–V compound semiconductor heterostructures, ultrahigh vacuum scanning tunneling microscopy (STM) performed in the cross-sectional geometry has proven to be particularly useful.[20–27]

In this article, we describe cross-sectional STM studies of compositional structure within alloy layers in $InAs_xP_{1-x}/InN_yAs_xP_{1-x-y}$/InP and $InAs_{1-x}P_x/InAs_{1-y}Sb_y$/InAs multiple-quantum-well and superlattice structures. $InAs_xP_{1-x}$/InP and, more recently, $InN_yAs_xP_{1-x-y}$/InP heterostructures are of interest for photodetectors and lasers operating at 1.06–1.55 μm.[28–32] The detailed compositional structure of the $InAs_xP_{1-x}$ and $InN_yAs_xP_{1-x-y}$ layers, within which both electrons and holes are confined in multiple-quantum-well structures, can directly and substantially influence the electronic and optical properties of such devices. $InAs_{1-x}P_x/InAs_{1-y}Sb_y$ superlattices coherently strained to InAs (001) are of current interest for mid- to long-wavelength infrared lasers. Evidence of atomic ordering has been observed in $InAs_{1-y}Sb_y$ alloys, with such ordering appearing to yield significant reductions in the energy band gap.[11] Understanding of and control over the compositional structure of this material system is therefore of critical importance.

II. EXPERIMENT

For these experiments an $InAs_xP_{1-x}/InN_yAs_xP_{1-x-y}$/InP sample was grown by gas-source molecular beam epitaxy (MBE). The sample structure consisted of a five-period 5 nm $InAs_{0.35}P_{0.65}$/10 nm InP multiple-quantum-well structure followed by a five-period 5 nm $InN_{0.01}As_{0.35}P_{0.64}$/20 nm InP multiple-quantum-well structure grown on an n^+-InP (001) substrate at a substrate temperature of 460 °C. Details of the gas-source MBE growth apparatus and growth procedures are described elsewhere.[33,34] The $InAs_{1-x}P_x/InAs_{1-y}Sb_y$ sample studied here was grown by metalorganic chemical vapor deposition (MOCVD), and consisted of a ten-period 9 nm $InAs_{0.73}P_{0.27}$/6.5 nm $InAs_{0.87}Sb_{0.13}$ superlattice grown on an InAs (001) substrate. Details of the MOCVD growth apparatus and growth procedures are described elsewhere.[35,36]

Samples were prepared for characterization by STM by

[a]Electronic mail: ety@ece.ucsd.edu

thinning wafer pieces to ~100–150 μm in thickness and subsequently cleaving them under ultrahigh vacuum conditions (7×10^{-11} Torr) to expose either a (110) or $(\bar{1}10)$ cross-sectional surface on which tunneling measurements were performed. While cleaving to expose both the (110) and $(\bar{1}10)$ cross-sectional planes yielded atomically flat surfaces suitable for characterization by STM, we found that cleaving to expose (110) planes was generally more successful. Constant-current imaging was performed in the STM using either commercially available Pt/Ir or electrochemically etched W tips cleaned *in situ* by electron bombardment.

III. RESULTS AND DISCUSSION

Constant-current STM images of the $InAs_{0.35}P_{0.65}/InP$ multiple-quantum-well structure reveal pronounced nanometer-scale inhomogeneities in composition within the $InAs_{0.35}P_{0.65}$ alloy. Figure 1 shows a schematic diagram of the $InAs_{0.35}P_{0.65}/InP$ sample structure, and filled-state STM images of the (110) and $(\bar{1}10)$ cross-sectional surfaces. Local, nanometer-scale variations in the electronic and, by extension, in the compositional structure are clearly visible, but with significantly different structure in the (110) and $(\bar{1}10)$ planes. In the (110) plane, local As-rich clusters (bright areas) are clearly visible. Furthermore, the boundaries between As-rich and P-rich (dark areas) regions appear to be oriented preferentially along the $[\bar{1}12]$ and $[1\bar{1}2]$ directions in the (110) plane. These directions represent the intersections of the cluster's boundary surfaces with the (110) plane. If the cluster boundary is taken to lie within a plane (*hkl*), the plane indexes must therefore satisfy the equation $h-k\pm2l=0$.

In the $(\bar{1}10)$ cross-sectional image in Fig. 1, local compositional variations are also visible; however, {112} boundaries between As-rich and P-rich regions are not in evidence. Instead, features appear to be aligned along the [110] direction in the crystal. For a planar cluster boundary (*hkl*), this observation indicates that the plane indexes must satisfy the equation $h+k=0$. The combined constraints on cluster boundary planes deduced from the (110) and $(\bar{1}10)$ cross-sectional images indicate that the cluster boundaries form preferentially within $(\bar{1}11)$ and $(1\bar{1}1)$ planes in the crystal, shown schematically in Fig. 2. Previous studies of $GaAs_{1-y}Sb_y$ alloys have revealed the presence of ordering on $(\bar{1}11)$ and $(1\bar{1}1)$ planes but not on (111) or $(11\bar{1})$ planes, and explained these observations as a consequence of surface reconstructions that occur during epitaxial growth.[3] The compositional structure we observe for $InAs_{0.35}P_{0.65}$ suggests that similar phenomena may occur during growth of $InAs_{0.35}P_{0.65}$, but that they influence the structure of boundaries formed between As-rich and P-rich clusters in the alloy rather than leading to the formation of fully ordered regions.

$InN_yAs_xP_{1-x-y}/InP$ multiple-quantum-well structures are of interest for lasers operating at 1.3–1.55 μm because of the reduction in strain and increase in conduction-band offset that result from N incorporation at low concentrations (a few percent or less). Photoluminescence characterization of $InN_yAs_xP_{1-x-y}/InP$ quantum-well structures with N con-

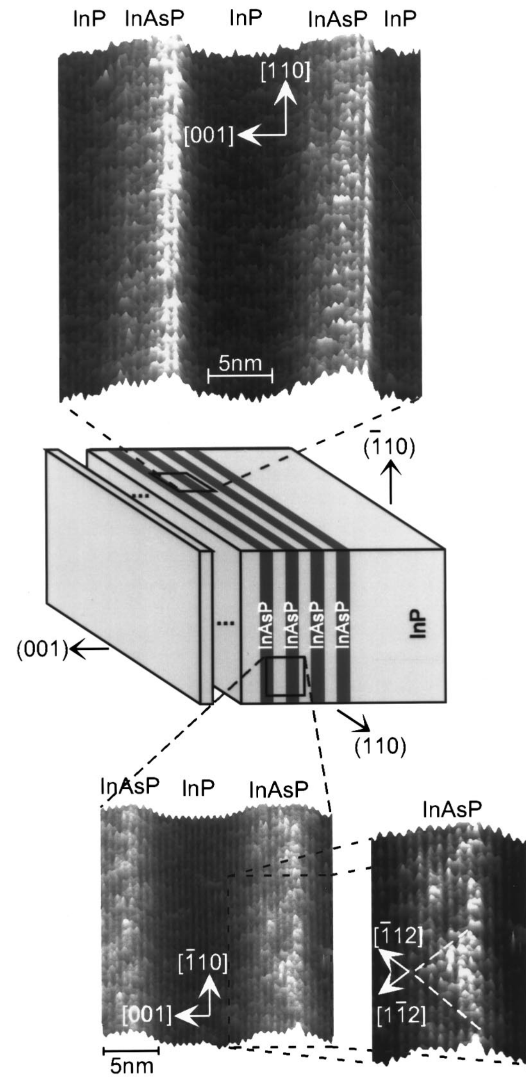

FIG. 1. Schematic diagram of the $InAs_{0.35}P_{0.65}/InP$ sample structure and filled-state constant-current images of the $(\bar{1}10)$ (top) and (110) (bottom) cross-sectional surfaces of a 5 nm $InAs_{0.35}P_{0.65}$/10 nm InP multiple-quantum-well structure showing As-rich (bright) and P-rich (dark) nanometer-scale clusters within the $InAs_{0.35}P_{0.65}$ alloy.

centrations of 0.7% and 3.7% has shown that N incorporation at low concentrations decreases the energy band gap of the $InN_yAs_xP_{1-x-y}$ alloys.[34] In addition, the large electronegativity of N suggests that N incorporation would tend to decrease the valence-band-edge energy in $InN_yAs_xP_{1-x-y}$ relative to that of $InAs_xP_{1-x}$.[32,34] The high-temperature performance observed for InNAsP/InGaAsP quantum-well lasers is, indeed, indicative of a large conduction-band offset that results from lowering of the $InN_yAs_xP_{1-x-y}$ conduction-band-edge energy.[32] Similar effects have been deduced theoretically[37,38] and experimentally[39] for low-concentration N incorporation into GaAs and InGaAs, respectively. While the combined effect of these influences will most likely be an increase in the conduction-band offset for the $InN_yAs_xP_{1-x-y}/InP$ heterojunction compared to that for $InAs_xP_{1-x}/InP$, the expected change in valence-band offset is less clear. Thus, information pertaining to the composi-

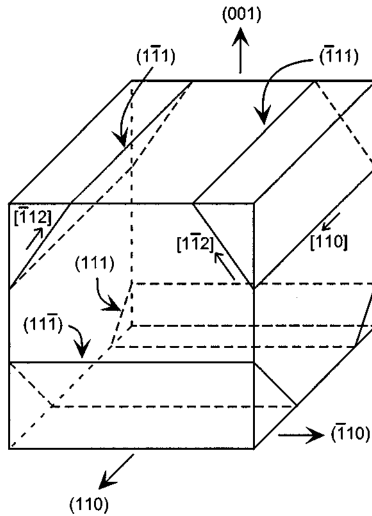

FIG. 2. Schematic diagram showing (001), (110), ($\bar{1}$10), and {111} crystal planes. Cluster boundaries forming within ($\bar{1}$11) and (1$\bar{1}$1) crystal planes will produce contrast aligned in the [1$\bar{1}$2] and [$\bar{1}$12] directions, respectively, in the (110) plane, and in the [110] direction in the ($\bar{1}$10) plane.

tional structure of the $InN_yAs_xP_{1-x-y}$ quantum-well layer and the band alignment for $InN_yAs_xP_{1-x-y}$/InP compared to that for $InAs_xP_{1-x}$/InP is of interest.

Figure 3 shows filled-state images of the (110) and ($\bar{1}$10) cross-sectional surfaces of a 5 nm $InN_{0.01}As_{0.35}P_{0.64}$/20 nm InP multiple-quantum-well structure obtained at a sample bias of −2.4 V and a tunneling current of 0.1 nA. For $InAs_{0.35}P_{0.65}$, $InN_{0.01}As_{0.35}P_{0.64}$, and InP layers contained within a single STM image, the contrast amplitude observed between $InN_{0.01}As_{0.35}P_{0.64}$ and InP was found to be larger than that between $InAs_{0.35}P_{0.65}$ and InP (typically ~2 and ~1.5 A, respectively). This observation suggests that the effect of increasing N incorporation at low concentrations is to increase the valence-band offset at the $InN_yAs_xP_{1-x-y}$/InP heterojunction interface. A similar trend has been predicted theoretically[38] for the GaN_yAs_{1-y}/GaAs valence-band offset when low concentrations of N are incorporated into GaAs.

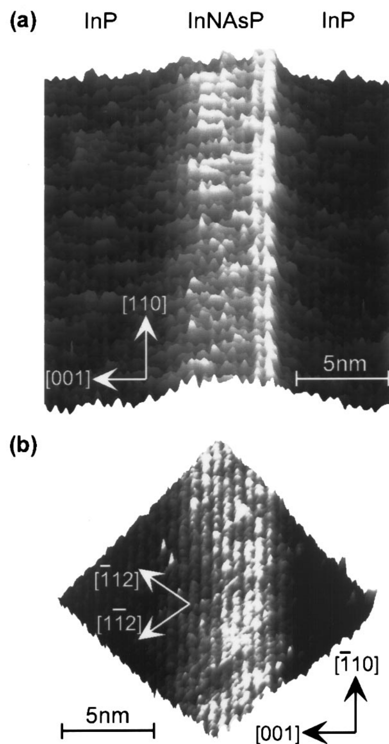

FIG. 3. Filled-state constant-current images of (a) the ($\bar{1}$10) and (b) the (110) cross-sectional planes of a 5 nm $InN_{0.01}As_{0.35}P_{0.64}$/20 nm InP multiple-quantum-well structure showing nanometer-scale compositional structure within the $InN_{0.01}As_{0.35}P_{0.64}$ alloy.

Examination of the images in Fig. 3 reveals a compositional structure in $InN_{0.01}As_{0.35}P_{0.64}$ similar to that found in $InAs_{0.35}P_{0.65}$. Boundaries between the bright and dark clusters in the $InN_{0.01}As_{0.35}P_{0.64}$ alloy are observed to be oriented preferentially along {112} directions in the (110) plane, and along the [110] direction in the ($\bar{1}$10) plane. These observations suggest that the cluster boundaries within $InN_{0.01}As_{0.35}P_{0.64}$ are contained preferentially within ($\bar{1}$11) and (1$\bar{1}$1) crystal planes, as was the case for the $InAs_{0.35}P_{0.65}$ alloy layers. Based on the expected influence of As, N, and P on the valence-band-edge energy, dark regions in the $InN_{0.01}As_{0.35}P_{0.64}$ alloy layer image are expected to be P rich, while bright regions may be As rich and/or N rich. Within the resolution of the images we have obtained of the $InN_{0.01}As_{0.35}P_{0.64}$ alloy layers, clear evidence of clustering of N atoms in the alloy is not observed, as has been seen for N incorporation into GaAs during MBE growth.[40]

Images of the (110) cross section of the $InAs_{0.73}P_{0.27}$/$InAs_{0.87}Sb_{0.13}$ superlattice structure grown on InAs (001) also show clear evidence of nanoscale compositional variations, but the details differ somewhat from those observed in $InAs_{0.35}P_{0.65}$ and $InN_{0.01}As_{0.35}P_{0.64}$ grown on InP described above. Figure 4 shows a filled-state image of the (110) cross section of the 9 nm $InAs_{0.73}P_{0.27}$/6.5 nm $InAs_{0.87}Sb_{0.13}$ superlattice structure. The $InAs_{0.87}Sb_{0.13}$ and $InAs_{0.73}P_{0.27}$ layers appear bright and dark, respectively, as expected on the basis of the valence-band-edge energy alignments at the $InAs_{0.87}Sb_{0.13}$/$InAs_{0.73}P_{0.27}$ heterojunction interface. Within the $InAs_{0.87}Sb_{0.13}$ layer, Sb-rich regions (bright) with typical dimensions of a few nanometers are clearly visible. There appears to be at most a limited preferential alignment of compositional features in this layer along the [$\bar{1}$12] direction. In the $InAs_{0.73}P_{0.27}$ alloy layer, P-rich (dark) regions are present that appear to be preferentially aligned along the [$\bar{1}$12] direction. Within the area shown in the image, only [$\bar{1}$12] features, corresponding to compositional variation along the [1$\bar{1}$1] direction, appear to be present. Previous studies of ordering in $InAs_{1-y}Sb_y$ alloys using transmission electron diffraction suggested that varying degrees of order along the [$\bar{1}$11] and [1$\bar{1}$1] directions were present in different locations within the sample; a similar phenomenon may be responsible for our observation of compositional variations primarily along the [1$\bar{1}$1] direction in our images. Closer examination of the $InAs_{0.73}P_{0.27}$ layer shown in Fig. 4 also reveals the presence of a region with P-rich and As-rich ma-

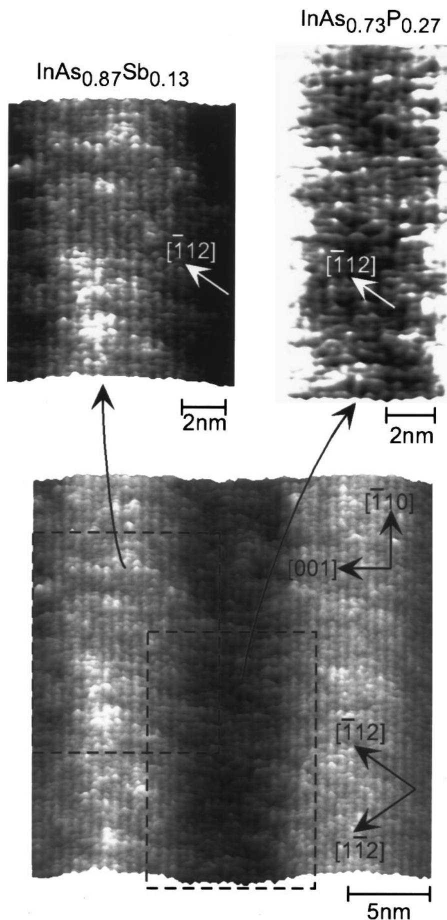

FIG. 4. Filled-state constant-current images of a 9 nm $InAs_{0.73}P_{0.27}$/6.5 nm $InAs_{0.87}Sb_{0.13}$ superlattice structure. Nanometer-scale compositional clustering is visible in both alloy materials.

terial alternating along the $[1\bar{1}1]$ direction with an approximate period of 2 nm. For pure CuPt ordering, the periodicity in compositional variation that would be observed would be approximately 0.7 nm, roughly one third that observed in the STM image.

Finally, we can observe in Fig. 5 that a correlation appears to exist between compositional features in adjacent alloy layers. Specifically, certain P-rich regions in the $InAs_{0.73}P_{0.27}$ layer appear to extend and merge with As-rich (dark) regions in the adjacent $InAs_{0.87}Sb_{0.13}$ layer, as indicated by the dark arrows in Fig. 5. The P-rich regions in $InAs_{0.73}P_{0.27}$ are under greater tensile strain than the alloy as a whole, while the As-rich regions in the $InAs_{0.87}Sb_{0.13}$ layer are under less compressive strain than the surrounding alloy layer. The correlation between the locations of these features in adjacent alloy layers suggests that local strain plays a significant role in the determination of compositional variations present in the alloy layers. Indeed, theoretical models of ordering in III–V alloys suggest that alloy ordering arises from strain-induced order in surface reconstructions present during growth that subsequently is incorporated into the structure of the epitaxially grown alloy.[41–43] Our observations are consistent with this model and suggest that, to some degree, such ordering can propagate across heterojunction interfaces.

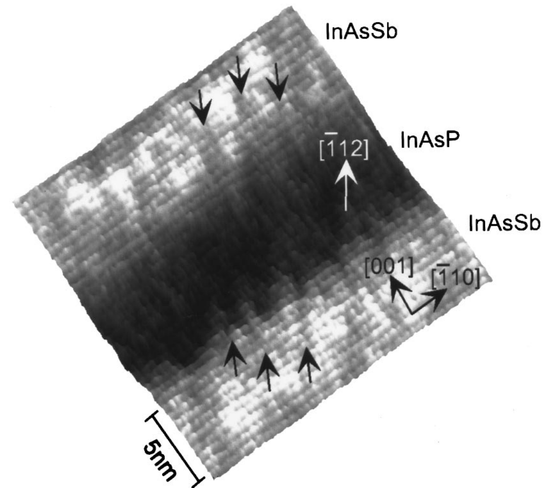

FIG. 5. Filled-state constant-current image of the $InAs_{0.73}P_{0.27}$/$InAs_{0.87}Sb_{0.13}$ superlattice structure showing (dark arrows) propagation across heterojunction interfaces of compositional clusters with similar strain relative to the surrounding alloy layers.

IV. CONCLUSIONS

We have performed detailed cross-sectional STM studies of the compositional structure in $InAs_xP_{1-x}$/$InN_yAs_xP_{1-x-y}$/InP and $InAs_{1-x}P_x$/$InAs_{1-y}Sb_y$/InAs heterostructures. Constant-current images reveal that nanoscale compositional variations are present in all alloy layers. For $InAs_xP_{1-x}$ and $InN_yAs_xP_{1-x-y}$ grown on InP (001), nanometer-scale compositional clustering is observed to occur, with boundaries between As-rich and P-rich regions forming preferentially within $(\bar{1}11)$ and $(1\bar{1}1)$ planes. For $InAs_{1-x}P_x$ and $InAs_{1-y}Sb_y$ grown on InAs (001), compositional clustering is also observed, with features appearing in the (110) plane suggesting that compositional variations have preferential orientations primarily along the $[1\bar{1}1]$ direction in the crystal. Instances of compositional structure correlated across a heterojunction interface are also observed, with regions whose composition corresponds to a smaller unstrained lattice constant relative to the surrounding alloy material appearing to propagate across a heterojunction interface. This observation is consistent with models in which alloy ordering arises from strain-induced order in surface reconstructions during epitaxial growth.

ACKNOWLEDGMENTS

The authors would like to acknowledge financial support from NSF (ECE 95-01469). One of the authors (E.T.Y.) would like to acknowledge financial support from the Alfred P. Sloan Foundation.

[1]T. S. Kuan, T. F. Kuech, W. I. Wang, and E. L. Wilkie, Phys. Rev. Lett. **54**, 201 (1985).
[2]H. R. Jen, M. J. Cherng, and G. B. Stringfellow, Appl. Phys. Lett. **48**, 1603 (1986).

[3]I. J. Murgatroyd, A. G. Norman, and G. R. Booker, J. Appl. Phys. **67**, 2310 (1990).
[4]M. A. Shahid, S. Mahajan, D. E. Laughlin, and H. M. Cox, Phys. Rev. Lett. **58**, 2567 (1987).
[5]A. Gomyo, T. Suzuki, and S. Iijima, Phys. Rev. Lett. **60**, 2645 (1988).
[6]A. Gomyo, K. Makita, I. Hino, and T. Suzuki, Phys. Rev. Lett. **72**, 673 (1994).
[7]G. B. Stringfellow and G. S. Chen, J. Vac. Sci. Technol. B **9**, 2182 (1991).
[8]A. Gomyo, K. Iobayashi, S. Kawata, I. Hino, T. Suzuki, and T. Yuasa, J. Cryst. Growth **77**, 367 (1986).
[9]S. H. Wei and A. Zunger, Phys. Rev. B **39**, 3279 (1989).
[10]D. J. Arent, M. Bode, K. A. Bertness, S. R. Kurtz, and J. M. Olson, Appl. Phys. Lett. **62**, 1806 (1992).
[11]S. R. Kurtz, L. R. Dawson, R. M. Biefeld, D. M. Follstaedt, and B. L. Doyle, Phys. Rev. B **46**, 1909 (1992).
[12]G. B. Stringfellow, J. Cryst. Growth **27**, 21 (1974).
[13]S. Mukai, J. Appl. Phys. **54**, 2635 (1983).
[14]G. B. Stringfellow, J. Cryst. Growth **65**, 454 (1983).
[15]A. G. Norman and G. R. Booker, J. Appl. Phys. **57**, 4715 (1985).
[16]S. N. G. Chu, S. Nakahara, K. E. Strege, and W. D. Johnston, Jr., J. Appl. Phys. **57**, 4610 (1985).
[17]I. T. Ferguson, A. G. Norman, B. A. Joyce, T.-Y. Seong, G. R. Booker, R. H. Thomas, C. C. Phillips, and R. A. Stradling, Appl. Phys. Lett. **59**, 3324 (1991).
[18]A. C. Chen, A. M. Moy, L. J. Chou, K. C. Hsieh, and K. Y. Cheng, Appl. Phys. Lett. **66**, 2694 (1995).
[19]J. Mirecki Millunchick, R. D. Twesten, D. M. Follstaedt, S. R. Lee, E. D. Jones, Y. Zhang, S. P. Ahrenkiel, and A. Mascarenhas, Appl. Phys. Lett. **70**, 1402 (1997).
[20]P. Muralt and D. W. Pohl, Appl. Phys. Lett. **48**, 514 (1986).
[21]H. W. M. Salemink, H. P. Meier, R. Ellialtioglu, J. W. Gerritsen, and P. R. M. Muralt, Appl. Phys. Lett. **54**, 1112 (1989).
[22]A. R. Smith, S. Gwo, K. Sadra, Y. C. Shih, B. G. Streetman, and C. K. Shih, J. Vac. Sci. Technol. B **12**, 2610 (1994).
[23]J. F. Zheng, J. D. Walker, M. B. Salmeron, and E. R. Weber, Phys. Rev. Lett. **72**, 2414 (1994).
[24]R. M. Feenstra, D. A. Collins, D. Z.-Y. Ting, M. W. Wang, and T. C. McGill, Phys. Rev. Lett. **72**, 2749 (1994).
[25]A. Y. Lew, E. T. Yu, D. H. Chow, and R. H. Miles, Appl. Phys. Lett. **65**, 201 (1994).
[26]S. L. Skala, W. Wu, J. R. Tucker, J. W. Lyding, A. Seabaugh, E. A. Beam III, and D. Jovanovic, J. Vac. Sci. Technol. B **13**, 660 (1995).
[27]E. T. Yu, Chem. Rev. **97**, 1017 (1997).
[28]E. Yablonovitch and E. O. Kane, J. Lightwave Technol. **6**, 1292 (1988).
[29]T. Fukushima, A. Kasukawa, M. Iwase, T. Namegaya, and M. Shibata, IEEE Photonics Technol. Lett. **5**, 117 (1993).
[30]T. K. Woodward, T.-H. Chiu, and T. Sizer II, Appl. Phys. Lett. **60**, 2846 (1992).
[31]H. Q. Hou, A. N. Cheng, H. H. Wieder, W. S. C. Chang, and C. W. Tu, Appl. Phys. Lett. **63**, 1833 (1993).
[32]W. G. Bi, Y. Ma, J. P. Zhang, L. W. Wang, S. T. Ho, and C. W. Tu, IEEE Photonics Technol. Lett. **9**, 1072 (1997).
[33]H. Q. Hou and C. W. Tu, Appl. Phys. Lett. **60**, 1872 (1992).
[34]W. G. Bi and C. W. Tu, Appl. Phys. Lett. **72**, 1161 (1998).
[35]R. M. Biefeld, K. C. Baucom, and S. R. Kurtz, J. Cryst. Growth **137**, 231 (1994).
[36]R. M. Biefeld, J. Cryst. Growth **75**, 255 (1986).
[37]S.-H. Wei and A. Zunger, Phys. Rev. Lett. **76**, 664 (1996).
[38]L. Bellaiche, S.-H. Wei, and A. Zunger, Phys. Rev. B **54**, 17568 (1996).
[39]M. Kondow, K. Uomi, A. Niwa, T. Kitatani, S. Watahiki, and Y. Yazawa, Jpn. J. Appl. Phys., Part 1 **35**, 1273 (1996).
[40]R. S. Goldman, R. M. Feenstra, B. G. Briner, M. L. O'Steen, and R. J. Hauenstein, Appl. Phys. Lett. **69**, 3698 (1996).
[41]S. Froyen and A. Zunger, Phys. Rev. Lett. **66**, 2132 (1991).
[42]S. Froyen and A. Zunger, Phys. Rev. B **53**, 4570 (1996).
[43]S. B. Zhang, S. Froyen, and A. Zunger, Appl. Phys. Lett. **67**, 3141 (1995).